2021 IEEE/RSJ International Conference on Intelligent Robots and Systems (IROS)
September 27 - October 1, 2021. Prague, Czech Republic

A Novel Quotient Space Approach to Model-Based Fault Detection and Isolation: Theory and Preliminary Simulation Evaluation

Annie M. Mao and Louis L. Whitcomb

2021 IEEE/RSJ International Conference on Intelligent Robots and Systems (IROS) | 978-1-6654-1714-3/21/$31.00 ©2021 IEEE | DOI: 10.1109/IROS51168.2021.9636026

***Abstract*— We report the development of novel fault detection and isolation (FDI) methods for model-based fault detection (MB-FD) and quotient-space fault isolation (QS-FI). This FDI approach performs MB-FD and QS-FI of single or multiple concurrent faults in plants and actuators simultaneously, without *a priori* knowledge of fault form, type, or dynamics. To detect faults, MB-FD characterizes deviation from nominal behavior using the plant velocity and plant and actuator parameters estimated by nullspace-based adaptive identification. To isolate (i.e. identify) faults, the QS-FI algorithm compares the estimated parameters to a nominal parameter class in progressively decreasing-dimensional quotient spaces of the parameter space. A preliminary simulation study of these proposed FDI methods applied to a three degree-of-freedom uninhabited underwater vehicle plant model shows their ability to detect as well as isolate faults for the cases of both single and multiple simultaneous faults and suggests the generalizability of the MB-FD and QS-FI approaches to any well-defined second-order plant and actuator model whose parameters enter linearly: a broad class of systems which includes aerial vehicles, marine vehicles, spacecraft, and robot arms.**

I. INTRODUCTION

Robots and autonomous vehicles hold incredible potential across all application areas for increasingly complex, long-endurance missions. In ocean science for example, the promise of robust and reliable robotic vehicles to advance human goals, reduce human danger, and expand human capabilities can hardly be overstated. The National Academy of Sciences (NAS) Ocean Studies Board's (OSB) Committee on an Ocean Infrastructure Strategy for U.S. Ocean Research in 2030 recently articulated the need for "extensive fleets of underwater gliders and autonomous underwater vehicles (AUVs) capable of operating in both expeditionary and long-duration modes... [and] AUVs with larger payloads, higher endurance, and ability to work in rough conditions (e.g. high currents, sea states, ice coverage) and at all expected working temperatures." [1]. Another study by the NAS OSB concluded "Unmanned vehicles (UVs)... are important to almost all decadal science priorities, demonstrating a broad utility across many scientific disciplines... UVs will continue to play a major role in providing detailed observations and enabling precise sampling, manipulative experiments, and installation of scientific equipment on the seafloor" [2].

The potential utility of robotic platforms, however, is vitiated by their vulnerability to unexpected faults. From changes in vehicle shape, mass, or buoyancy, to actuator failure, to external disturbance, faults are difficult to detect, isolate, and – when possible – compensate for. While some subsystems directly report fault status (e.g. a vehicle power distribution system continuously monitoring for ground-faults in onboard electric instruments), many plant and actuator faults can only be inferred by observing the effect of control input on the dynamic response of a vehicle. For example, no sensors onboard an uninhabited underwater vehicle (UUV) are able to detect directly an unexpected change in vehicle mass or buoyancy. Consequences range from aborted or failed missions to total loss of vehicle and collateral damage. The success of future robot systems, especially as application spaces expand to less controlled and predictable environments, depends highly on effective fault detection and isolation (FDI) and fault-tolerant control.

This paper reports a novel model-based fault detection (MB-FD) method and a novel quotient-space fault isolation (QS-FI) algorithm and evaluates their performance in numerical simulations. The MB-FD methods utilizes recent advancements in adaptive identification (AID) of dynamical model parameters, namely nullspace-based adaptive identification (NS-AID) [3]. To the best of our knowledge, this is the first application of NS-AID to perform FDI. Without needing to make any assumptions about potential fault dynamics, this approach detects fault conditions via any change in the underlying model parameters that causes a deviation from nominal vehicle behavior. We also report a novel QS-FI algorithm that determines which parameters are responsible for the fault by exploiting the linearity of the parameters in the system dynamics. A simulation study using a three-degree-of-freedom (3-DOF) UUV plant model shows the ability of this FDI approach to detect as well as isolate faults for the cases of both single and multiple simultaneous faults and suggests its generalizability to the broad class of second-order dynamical systems whose plant and actuator parameters enter linearly, e.g. aerial vehicles, marine vehicles, spacecraft, and robot arms.

II. RELATED WORK

In 2015, an exhaustive survey of the field by Gao, Cecati, and Ding identified five broad categories of FDI: model-based, signal-based, knowledge-based, active, and hybrid approaches [4], [5]. Model-based methods are applicable to dynamical systems whose continuous-time or discrete-time dynamics are known *a priori*. Signal-based methods apply statistical signature tests and/or spectrum analysis to plant input and output signals to distinguish between normal and fault conditions, e.g. [6]. Knowledge-based methods, in lieu

We gratefully acknowledge the support of the first author by Graduate Fellowships from the Johns Hopkins University Department of Mechanical Engineering, Laboratory for Computational Sensing and Robotics, and Applied Physics Laboratory; as well as the support of the National Science Foundation under award IIS-1909182.

The authors are with the Department of Mechanical Engineering, Johns Hopkins University, Baltimore, MD 21218, USA amao1@jhu.edu, llw@jhu.edu

of plant models or signal patterns, rely on historical data sets from past plant operations, e.g. [7]. Machine learning approaches such as [8], [9] fall into this category. Active methods seek to discern normal or fault conditions from *a priori* known responses in the plant output to additive probe signals applied on the plant input, e.g. [10]. Hybrid methods involve some combination of the above approaches, e.g. [11].

Of the 227 papers cited in the 2015 survey papers by Gao, Cecati, and Ding, less than 10% address FDI for uninhabited or autonomous systems [4], [5], and effective fault detection and fault-tolerant control remain open problems in robotics, posing significant obstacles to reliable deployments. A study by the developers of the *Tethys* long-range UUV of 7,000 hours of mission time reported 199 faults that required the vehicle to surface unexpectedly [12]. Of these 199 faults, 119 arose from servo/thruster faults. Studies of the *ABE* AUV [13], [14] and the *Sentry* AUV [15] by the NSF-supported National Deep Submergence Facility of the *ABE's* and *Sentry's* first 380 scientific dive missions revealed that 68 of the 380 missions terminated prematurely due to faults. Of these 68 failed missions, 43 failures (or 63%) were due to plant or actuator faults of the type addressed herein [16]. Other AUV groups report similar fault statistics, e.g. [17], [18], [19]. Clearly, the need for more effective fault detection and isolation – leading to more effective fault mitigation and fault-tolerant control – remains a key obstacle to the success of robotics applications in the real world.

Among model-based FDI approaches, residual-based solutions have been widely explored. Regarding faults as inputs acting on the system, such approaches seek to generate a set of residual outputs that isolate the faults, where each residual filters for one fault independently of all other inputs. The selective sensitivity of each residual then enables detection and isolation of multiple concurrent faults. Notably, Massoumnia derived necessary and sufficient conditions for the solvability of the residual generation problem, formulated as the construction of a Luenberger observer [20], and De Persis and Isidori generalized these results to nonlinear systems [21]. Another class of methods applies parameter identification techniques such as least squares [22] and adaptive identification [23] to estimate the parameters of a model of the fault included in the system dynamics; these estimates then serve as the residual signals.

All of the above approaches fundamentally assume knowledge of fault dynamics, explicitly modeling every potential fault as an input to the system, e.g. as additive torques [22]. In contrast, we propose an approach that performs parameter identification not on an assumed fault model, but directly on the model of the plant and actuator. By defining faults not as separate inputs to the system, but as any change in the underlying plant and actuator parameters that govern system behavior, our approach enables fault detection and insight into the fault source without specifying its form *a priori*. Moreover, adaptive online estimation of the true plant and actuator parameters to capture the behavior of the system accurately even under fault conditions then provides a natural basis for fault-tolerant control.

Model-based approaches to a wide range of problem in robotics have motivated extensive work in nonlinear system identification, since they require exact knowledge of the plant's kinematic and dynamic parameters. While kinematic parameters are often easily measurable and generally do not vary with time, plant dynamic parameters are often subject to change, either from external disturbance (e.g. bio-fouling of a underwater vehicle hull increasing its drag), vehicle reconfiguration (e.g. the mass and inertial distribution of a vehicle varying with different payloads), or even routine operation (e.g. decreasing mass from fuel consumption). These dynamic parameters must be identified through empirical experimentation. Most previously reported identification methods for parameters entering linearly into the plant equations of motion employ least squares [24], [25], [26], [27], [28], Kalman filter [29], [30], machine learning [31], [32], [33], [34], or adaptive [35], [36] methods.

In [3], Paine reported a novel nullspace-based adaptive identifier (NS-AID) for simultaneous estimation of both plant and actuator parameters, discussed further in Sections IV-A and V-B. Unlike many previous parameter identification approaches, the NS-AID does not require *a priori* knowledge of the actuator parameters, requires access only to position and velocity signals and does not require instrumentation of acceleration, converges quickly enough for online estimation, and has been applied to both fully actuated and underactuated systems [3]. In the present study, we apply a NS-AID to the FDI problem, systematically characterizing the behavior of the system through parameter estimation. To the best of our knowledge, this paper reports the first application of an adaptive identifier for fault detection via simultaneous plant and actuator model parameter estimation, as well as a novel algorithm for fault isolation via quotient space-based analysis of the model parameter vector.

III. PROBLEM STATEMENT

We consider the general class of n degree-of-freedom second-order nonlinear systems of the form

$$G_a(\xi)\theta_a \quad = \quad W_p(\dot{v}, v, q)\theta_p \tag{1}$$

where $q \in \mathbb{R}^n$ are the world-frame position and attitude coordinates, $v, \dot{v} \in \mathbb{R}^n$ are body-frame velocities and accelerations, respectively, and $\xi \in \mathbb{R}^c$ is the control input. The plant model on the right-hand side of (1) consists of the matrix-valued function $W_p(\dot{v}, v, q) \in \mathbb{R}^{n \times p}$ (termed the "regressor matrix") and a parameter vector $\theta_p \in \mathbb{R}^p$ representing the plant dynamic coefficients such as mass, inertia, lift, drag, or buoyancy terms. $W_p(\dot{v}, v, q)$ can be determined from kinematic analysis, whereas θ_p must be determined empirically. Similarly, the left-hand side of (1) shows the actuator model, factored into the matrix-valued function $G_a(\xi)$ and the actuator parameter vector $\theta_a \in \mathbb{R}^a$, which contains thruster, propeller, control surface or other actuator coefficients. This broad class of systems whose parameters enter linearly includes marine and aerial vehicles [37], spacecraft [38], and robot arms [39].

Combining the plant and actuator dynamics, we have

$$0 = [W_p(\dot{v}, v, q) \ -G_a(\xi)] \begin{bmatrix} \theta_p \\ \theta_a \end{bmatrix} \quad (2)$$

$$= W_{pa}(\dot{v}, v, q, \xi)\theta_{pa} \quad (3)$$

where the aggregate vector of plant and actuator parameters $\theta_{pa} = [\theta_p^T \ \theta_a^T]^T \in \mathbb{R}^{(p+a)}$ is a member of the nullspace of the known time-varying regressor matrix-valued function $W_{pa}(\dot{v}, v, q, \xi) = [W_p(\dot{v}, v, q), -G_a(\xi)] \in \mathbb{R}^{n\times(p+a)}$. This means that the "true" parameter vector is not a single point in parameter space $\mathbb{R}^{p+a}$, but an element of the equivalence class $P \subset \mathbb{R}^{(p+a)}$. P is a linear vector subspace of $\mathbb{R}^{(p+a)}$ defined as

$$P = \{\theta_{pa} : \|\theta_{pa}\| \neq 0, \forall t \ \ \theta_{pa} \in \text{null}(W_{pa}(\dot{v}, v, q, \xi))\}. \quad (4)$$

In other words, each equivalence class P represents all parameter vectors that belong to a particular evolution of $W_{pa}(\dot{v}, v, q, \xi)$ over time. We note that this nullspace structure arises from the linearity of the parameter vector in the equations of motion of this class of systems and not from any artifact of the FDI methods we later employ; for example, (1) remains invariant for any scalar multiple of the entire parameter vector θ_{pa}.

Given some nominal P^* corresponding to a "known good" or expected set of system behaviors, we can represent the "true" parameter vector as

$$\theta_{pa} = \theta^*_{pa} + \eta \quad (5)$$

where $\theta^*_{pa} \in P^*$ is the nominal part and $\eta \notin P^*$ is an unknown deviation. Our goal is then to detect the presence of nontrivial η, i.e. a fault, and to isolate its source by determining the specific plant and actuator parameters affected.

IV. MODEL-BASED FAULT DETECTION AND QUOTIENT-SPACE FAULT ISOLATION

We have seen above that each equivalence class of parameter vectors (4) "belongs" to a set of system behaviors, i.e. the nullspace of the regressor matrix-valued function. Identifying the parameter vector corresponding to the system's motion at any given point can thus serve to characterize its normal or fault condition. This FDI approach employs a novel application of nullspace-based adaptive identification (NS-AID) as described in [3] to compute estimates of plant and actuator parameters simultaneously, which then serve as inputs to the MB-FD and QS-FI methods described below.

A. Online Stable Nullspace-Based Adaptive Identification

With the assumptions that the state $q(t)$, velocity $v(t)$, and control input $\xi(t)$ are available signals, but without requiring access to acceleration, the NS-AID computes an online estimate $\hat{\theta}_{pa}(t)$ of the plant and actuator parameters, as well as an estimated velocity $\hat{v}(t)$ based on $\hat{\theta}_{pa}(t)$. We define the error coordinates

$$\Delta v(t) = \hat{v}(t) - v(t) \quad (6)$$

$$\Delta\theta_{pa}(t) = \hat{\theta}_{pa}(t) - \theta_{pa}(t). \quad (7)$$

As shown in [3], we can then design update laws $\dot{\hat{v}}(t)$, $\dot{\hat{\theta}}_{pa}(t)$ such that all signals remain bounded, $\lim_{t\to\infty} \Delta v(t) = \vec{0}$, $\lim_{t\to\infty} \dot{\hat{\theta}}_{pa}(t) = \vec{0}$ and, with additional persistence of excitation (PE) conditions[1], $\lim_{t\to\infty} \hat{\theta}_{pa}(t) \in P$.

The strong stability and convergence properties of these signals provide insight into system behavior that is robust against noise and disturbance. In the following section, we will employ these signals as the basis of our FDI approach.

B. Fault Detection and Isolation

During vehicle operation, continuous estimation of the vehicle velocity and plant and actuator parameters by the NS-AID enables both the detection of abnormal vehicle behavior and the isolation of a fault to the parameters responsible.

1) Model-Based Fault Detection (MB-FD)

The velocity and parameter estimates of the NS-AID can indicate the presence of a fault in two distinct ways. First, we expect that the magnitude of the error $\Delta v(t) = \hat{v}(t) - v(t)$ between the estimated and true vehicle velocities should be large at the beginning of a mission and converge to a small value as the AID correctly identifies the vehicle plant and actuator parameters. Any significant increase in the magnitude of $\Delta v(t)$ after the initial convergence period indicates an unexpected change in the underlying parameters of the system and thus existence of one or more faults, but does not reveal the cardinality or nature of the faults.

Second, we can continuously compute a separate real-time forward simulation of the vehicle velocity, denoted $v_{\theta_{pa^*}}$, according to (1) and an *a priori* known good set of nominal parameters $\theta_{pa^*} \in P^*$ identified from previous vehicle trials or from the first converged estimate. The magnitude of the error $\Delta v_{\theta_{pa^*}}(t) = v_{\theta_{pa^*}}(t) - v(t)$ reflects the deviation of vehicle behavior from the nominal known good as in 5, and any significant increase again indicates one or more faults but does not isolate their cause. Unlike $\Delta v(t)$, this error persists even after re-convergence of the NS-AID.

For both of these fault detection metrics, it is necessary to tune the error threshold based on empirical data for the system being considered to mitigate false positives due to fluctuations of the NS-AID during estimation.

2) Quotient-Space Fault Isolation (QS-FI)

While the plant velocity estimated by the NS-AID can be directly compared to a true or nominal velocity to detect the *presence* of a fault, as above, it is not as simple to isolate the source of the fault. Because each parameter vector is not a single point but a member of an equivalence class, the absolute error between any two sets of parameters is not well-defined; for example, it could be confounded by the possibly different scale factors.

A more meaningful error metric, given a nominal $\theta_{pa^*} \in P^*$ and test vector $\hat{\theta}_{pa}$, is the projection of $\hat{\theta}_{pa}$ onto $P^{*\perp}$, the orthogonal complement of the equivalence class P^* to which θ_{pa^*} belongs. Persistent nonzero values of $\hat{\theta}_{pa} \in P^{*\perp}$ certainly signal a fault via the deviation of $\hat{\theta}_{pa}$ from the

[1]The signal W(t) is PE if $\exists$ constants $t_o, T > 0, \text{and}\, \epsilon > 0$ such that $\forall t > t_o$, it holds that $\sigma_{min}[\int_t^{t+T} W(\tau)^T W(\tau) d\tau] \geq \epsilon$, where the $\sigma_{min} : \mathbb{R}^{n\times n} \to \mathbb{R}$ returns the smallest eigenvalue of the positive symmetric real argument [40], [41].

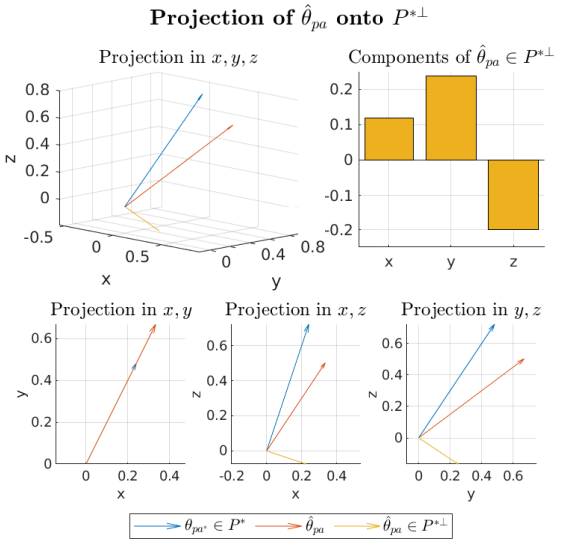

Fig. 1. Comparing a "fault" parameter vector $\hat{\theta}_{pa}$ to a "nominal" parameter vector θ_{pa^*} (both shown as normalized unit vectors) by projecting $\hat{\theta}_{pa}$ onto $P^{*\perp}$, the orthogonal complement of $span\{\theta_{pa^*}\}$. The fault in $\hat{\theta}_{pa}$ consists of a 50% reduction of the z-component, which is obscured when looking directly at the components of $\hat{\theta}_{pa} \in P^{*\perp}$ (top right). However, viewing $\hat{\theta}_{pa}, \theta_{pa^*}$ in the quotient spaces created by collapsing one dimension at a time (bottom) reveals the z-dimension to be the source of the fault.

nominal subspace, and one potential method to localize the responsible parameters is to examine the components of $\hat{\theta}_{pa} \in P^{*\perp}$. But because a change in any individual component of the parameter vector moves the entire vector in parameter space $\mathbb{R}^{p+a}$, the real source of the fault remains obscured. Figure 1 shows an example of a 3D nominal parameter vector $\theta_{pa*} = [1\ 2\ 3]^T$ and estimated "true" parameters with a fault in the z-dimension, $\hat{\theta}_{pa} = [1\ 2\ 1.5]^T$, which have been normalized to reflect that parameter vectors are unique up to a scale factor. We see that, although the z-parameter is solely responsible for the fault, the components of $\hat{\theta}_{pa} \in P^{*\perp}$ show a higher "error" value in the y dimension. Notably, however, when $\theta_{pa^*}, \hat{\theta}_{pa}$ are projected onto the xy-plane, $\hat{\theta}_{pa}$ now appears to lie exactly within the span of θ_{pa^*}. In other words, when the faulty parameters are quotiented out of the parameter vector, the fault is no longer detectable.

Using this basic intuition, the fault isolation algorithm (Algorithms 1 and 2) determines the fault source by collapsing progressively increasing dimensions of the parameter space, testing for the combination of dimensions in which $\theta_{pa^*}, \hat{\theta}_{pa}$, belong to the same equivalence class. Then the excluded dimensions must be the source of the fault. In linear algebraic terms, for every combination C_k of k standard basis vectors $\{e_{i \in C_k}\}$ (Alg. 2 Line 3) we map $\theta_{pa^*}, \hat{\theta}_{pa}$ to elements $q^*, \hat{q}$ of the quotient space $Q := \mathbb{R}^{p+a}/sp\{e_{i \in C_k}\}$, which is isomorphic to $\mathbb{R}^{(p+a)-k}$ (Alg. 2 Line 4). If the projection of $\hat{q}$ onto the orthogonal complement of $sp\{q^*\}$ performed in the quotient space has magnitude less than some error threshold $\epsilon > 0$, we have found a fault-free parameter subspace (Alg. 2 Line 9). Starting with all combinations of $\binom{p+a}{1}$ dimensions, we progressively quotient more and more dimensions (Alg. 1 Line 5) until the first fault-free subspace is found. Then the k excluded dimensions are the source of a fault of k concurrent parameters (Alg. 1 Line 11). As with the MB-FD, the error threshold ϵ must be determined empirically based on the system in question.

Algorithm 1 Fault isolation algorithm

1: **procedure** FIND_FAULT($\theta^*_{pa}, \hat{\theta}_{pa}$)
2: $flags \leftarrow [-1, -1, ..., -1]^T \in \mathbb{R}^{p+a}$
3: ▷ Start with $(p+a)-1$ combinations
4: $k \leftarrow 1$
5: ▷ Collapse the parameter space into progressively lower dimensions until a fault is found or the threshold of faults to be considered simultaneously has been reached
6: **while** $k <= k_{max}$ **do**
7: $i_{good} \leftarrow$ PROJ_QUOTIENT_K($\theta^*_{pa}, \hat{\theta}_{pa}, k$)
8: **if** $i_{good} = \emptyset$ **then**
9: ▷ Keep looking in lower dimensions
10: $k \leftarrow k + 1$
11: **else**
12: ▷ Found fault; indicate fault locations
13: $i_{bad} = \{1, ..., (p+a)\} \setminus i_{good}$
14: $flags[i_{good}] \leftarrow 0$ ▷ no-fault parameters
15: $flags[i_{bad}] \leftarrow k$ ▷ k-fault parameters
16: **end if**
17: **end while**
18: **return** $flags$
19: **end procedure**

Algorithm 2 Projection of estimated $\hat{\theta}_{pa}$ and nominal θ^*_{pa} onto quotient spaces of the parameter space

1: **procedure** PROJ_QUOTIENT_K($\theta^*_{pa}, \hat{\theta}_{pa}$,k)
2: $i_{good} \leftarrow \emptyset$
3: **for all** $\binom{p+a}{k}$ combinations C_k of $1, ..., (p+a)$ **do**
4: ▷ Map $\theta_{pa^*}, \hat{\theta}_{pa}$ to $Q := \mathbb{R}^{p+a}/sp\{e_{i \in C_k}\}$
5: $q^* \leftarrow \theta^*_{pa}[i \notin C_k]$
6: $\hat{q} \leftarrow \hat{\theta}_{pa}[i \notin C_k]$
7: ▷ Normalize $q^*, \hat{q}$
8: ▷ Project $\hat{q}$ onto $sp(q^*)^\perp$
9: $E \leftarrow (I_{(p+a)-k} - q^*(q^*)^T)\hat{q}$
10: **if** $||E||_2 < \epsilon$ **then**
11: ▷ Found a fault-free subspace
12: $i_{good} \leftarrow i_{good} \cup i \notin C_k$
13: **end if**
14: **end for**
15: **return** i_{good}
16: **end procedure**

This fault isolation method has algorithmic complexity $\mathcal{O}((p+a)^{k_{max}})$ due to the $\binom{p+a}{k}$ combinations at each level k. Heuristic methods for first considering groupings of parameters (e.g. all mass parameters or all drag parameters) to narrow the search space offer significant potential for efficiency gains. Finally, separating fault detection and fault isolation into a two-stage process by attempting fault

isolation only upon triggering a fault detection event can further reduce computational expense.

V. PRELIMINARY SIMULATION STUDY IN 3-DOF

To investigate the feasibility of the novel MB-FD and QS-FI algorithms introduced in Section IV, we conducted a simulation study of the proposed approaches applied to a 3-DOF UUV plant model. We note that, while this preliminary study was performed on a limited underwater vehicle model, the mathematical principles central to the FDI approach depend only on the linearity of the parameters in the system dynamics and are thus applicable to any system that can be written in the form (1) – including a wide variety of aerial, marine, space, and manipulator platforms. Furthermore, NS-AID employed to provide parameter estimates to the FDI algorithms has been studied for both fully-actuated and underactuated 3-DOF and 6-DOF UUV models under noise conditions, indicating high potential for generalizability.

A. 3-DOF Dynamical Plant Model

As derived in [3], we have the following equations of motion for a general 3-DOF UUV

$$\tau(v,\xi) \quad = \quad M\dot{v} + C(v)v + D(v)v + \mathcal{G}(q). \tag{8}$$

The UUV hydrodynamic model is the right-hand side of (8), where $M \in \mathbb{R}^{3\times3}$ is the positive-definite symmetric vehicle mass matrix, $C(v) \in \mathbb{R}^{3\times3}$ is the vehicle Coriolis matrix-valued function, $D(v) \in \mathbb{R}^{3\times3}$ is the positive semi-definite quadratic drag matrix-valued function $D(v) = \sum_{i=1}^{3} |v_i|D_i$, and $\mathcal{G}(q) \in \mathbb{R}^3$ is the buoyancy/gravity force/moment vector. The control vector $\tau(v,\xi) \in \mathbb{R}^3$ is defined as the body forces resulting from body velocity v and a control input vector denoted as $\xi \in \mathbb{R}^3$. For this preliminary study, we choose the body center-of-mass (COM) frame.

To write the system in the form of (1), we factor the right-hand side of (8) as

$$M\dot{v} + C(v)v + D(v)v + \mathcal{G}(q) = W_p(\dot{v}, v, q)\theta_p, \tag{9}$$

the product of the regressor matrix and and the parameter vector θ_p containing the plant hydrodynamic coefficients.

For this 3-DOF model in the vertical plane (surge, heave, and pitch), the factorization in (9) yields a 25-parameter plant model as follows:

$$M\dot{v} = \begin{bmatrix} {}^bM_T & 0_{2\times1} \\ 0_{1\times2} & {}^bi \end{bmatrix}\dot{v} = \begin{bmatrix} m_{11} & m_{12} & 0 \\ m_{12} & m_{22} & 0 \\ 0 & 0 & m_{33} \end{bmatrix}\dot{v} \tag{10}$$

$$= W_{p_M}(\dot{v})\theta_{p_M} \tag{11}$$

where ${}^bM_T \in \mathbb{R}^{2\times2}$ represents the combined hydrodynamic and rigid body added mass and ${}^bi \in \mathbb{R}$ represents the hydrodynamic and rigid body rotational inertia. Then $\theta_{p_M} = [m_{11}\ m_{12}\ m_{22}\ m_{33}]^T \in \mathbb{R}^4$ parameterizes both the mass matrix as in (11) and the Coriolis matrix as in (13):

$$C(v)v = \begin{bmatrix} 0_{2\times2} & \mathcal{J}^T(1)\ {}^bM_T \begin{bmatrix} v_1 \\ v_2 \end{bmatrix} \\ [v_1\ v_2]\ {}^bM_T\mathcal{J}^T(1) & 0 \end{bmatrix} v \tag{12}$$

$$= ad_{se(2)}(v)W_{p_M}(v)\theta_{p_M} \tag{13}$$

where we define the adjoint operator $ad_{se(2)} : \mathbb{R}^3 \to \mathbb{R}^{3\times3}$

$$ad_{se(2)}(v) = \begin{bmatrix} 0 & v_3 & 0 \\ -v_3 & 0 & 0 \\ v_2 & -v_1 & 0 \end{bmatrix} \tag{14}$$

and the skew-symmetric operator $\mathcal{J} : \mathbb{R}^{\to}\mathbb{R}^{2\times2}$

$$\mathcal{J}(a) = \begin{bmatrix} 0 & -a \\ a & 0 \end{bmatrix}. \tag{15}$$

The drag matrix for each DOF, herein defined positive semi-definite symmetric and signed appropriately as a dissipative term, is given by:

$$D_i = \begin{bmatrix} d_{11} & d_{12} & d_{13} \\ d_{12} & d_{22} & d_{23} \\ d_{13} & d_{23} & d_{33} \end{bmatrix} \tag{16}$$

so that $\theta_{p_{D_i}} = [d_{11}\ d_{12}\ d_{13}\ d_{22}\ d_{23}\ d_{33}]^T \in \mathbb{R}^6$ and the stacked vector $\theta_{p_D} = [\theta_{p_{D_1}}^T\ \theta_{p_{D_2}}^T\ \theta_{p_{D_3}}^T]^T \in \mathbb{R}^{18}$ parameterizes the total quadratic drag

$$D(v)v = (\sum_{i=1}^{3} |v_i|D_i)v = W_{p_D}(v)\theta_{p_D}. \tag{17}$$

We define $r_{cb} = [r_{cb,x}\ r_{cb,z}]^T \in \mathbb{R}^2$ as the vector from the body COM to the center of buoyancy. Then $\mathcal{G}(q)$ consists of the force ${}^bf_{\mathcal{G}} \in \mathbb{R}^2$ and the righting moment ${}^b\tau_{\mathcal{G}} \in \mathbb{R}$ exerted on the vehicle by gravity and the buoyant forces, written as follows, where $R(q) \in SO(2)$ is the rotation from the world to the body frame, $\rho, m, \bigtriangledown$ are the water density, vehicle dry mass, and vehicle displacement volume, respectively, $e_2 = [0\ 1]^T$, and g_c is the gravitational constant:

$$\mathcal{G}(q) = \begin{bmatrix} {}^bf_{\mathcal{G}} \\ {}^b\tau_{\mathcal{G}} \end{bmatrix} = \begin{bmatrix} g_cR(q)e_2(m - \rho\bigtriangledown) \\ g_cr_{cb}^T\mathcal{J}(1)Re_2(-\rho\bigtriangledown) \end{bmatrix} \tag{18}$$

$$= W_{p_{\mathcal{G}}}(q)\theta_{p_{\mathcal{G}}}, \tag{19}$$

with parameters $\theta_{p_{\mathcal{G}}} = [m - \rho\bigtriangledown\ \ r_{cb,x}\rho\bigtriangledown\ \ r_{cb,z}\rho\bigtriangledown]^T \in \mathbb{R}^3$.

Combining (11),(13),(17),(19) gives the regressor matrix

$$W_p(\dot{v}, v, q) = \\ [(W_{p_M}(\dot{v}) + ad_{se(2)}(v)W_{p_M}(v))\ \ W_{p_D}(v)\ \ W_{p_{\mathcal{G}}}(q)] \tag{20}$$

and parameter vector $\theta_p = [\theta_{p_M}^T\ \theta_{p_D}^T\ \theta_{p_{\mathcal{G}}}^T]^T \in \mathbb{R}^{25}$.

We use a simple actuator model with three thrusters, whose forces in the direction of unit vectors $u_1, u_2, u_3 \in \mathbb{R}^3$ are proportional to the signed square of the control inputs $\xi_1, \xi_2, \xi_3 \in \mathbb{R}$ with proportionality constants $\alpha_1, \alpha_2, \alpha_3 \in \mathbb{R}$, located with respect to the body COM frame by $r_{a_1}, r_{a_2}, r_{a_3} \in \mathbb{R}^2$. Then we can express the external forces and moments $\tau(v,\xi)$ in (8) as follows:

$$\tau(v,\xi) = \begin{bmatrix} {}^b f_a \\ {}^b \tau_a \end{bmatrix} = \begin{bmatrix} \sum_{i=1}^{3} \alpha_i \xi_i |\xi_i| u_i \\ \sum_{i=1}^{3} \alpha_i \xi_i |\xi_i| r_{a_i} \times u_i \end{bmatrix} \quad (21)$$

$$= \begin{bmatrix} a_{11} & a_{12} & a_{13} \\ a_{21} & a_{22} & a_{23} \\ a_{31} & a_{32} & a_{33} \end{bmatrix} \begin{bmatrix} \xi_1|\xi_1| \\ \xi_2|\xi_2| \\ \xi_3|\xi_3| \end{bmatrix} \quad (22)$$

$$= G_a(\xi)\theta_a \quad (23)$$

with parameter vector $\theta_a = [a_{11}\ a_{12}\ a_{13}...a_{33}]^T \in \mathbb{R}^9$. The combined plant and actuator parameter vector can thus be constructed as $\theta_{pa} = [\theta_p^T\ \theta_a^T]^T \in \mathbb{R}^{34}$

B. Online Stable Adaptive Plant and Actuator Parameter Identification

Following the approach reported in ([3]), we design the following parameter update laws for the NS-AID:

$$\dot{\hat{v}} = \hat{M}^{-1}(-\hat{C}(v)v - \hat{D}(v)v + \hat{\mathcal{G}}(q) + G_a(\xi)\hat{\theta}_a) - \alpha\Delta v \quad (24)$$

$$\dot{\hat{\theta}}_{p_M} = \gamma_M(\psi_1^T W_{p_M}(v) + \psi_2^T W_{p_M}(\Delta v)) \quad (25)$$

$$\dot{\hat{\theta}}_{p_{D_1}} = \gamma_{D_1}(W_{p_{D_1}}(v))^T \Delta v \quad (26)$$

$$\dot{\hat{\theta}}_{p_{D_2}} = \gamma_{D_2}(W_{p_{D_2}}(v))^T \Delta v \quad (27)$$

$$\dot{\hat{\theta}}_{p_{D_3}} = \gamma_{D_3}(W_{p_{D_3}}(v))^T \Delta v \quad (28)$$

$$\dot{\hat{\theta}}_{p_\mathcal{G}} = -\gamma_\mathcal{G}(W_{p_\mathcal{G}}(q))^T \Delta v \quad (29)$$

$$\dot{\hat{\theta}}_a = -\gamma_a(G_a(\xi))^T \Delta v \quad (30)$$

where

- $\psi_1 = ad_{se(2)}(v)^T \Delta v$
- $\psi_2 = \dot{\hat{v}} + \alpha\Delta v$
- α, γ_M, γ_{D_1}, γ_{D_2}, γ_{D_3}, $\gamma_\mathcal{G}$, $\gamma_a \in \mathbb{R}_+$
- $\hat{v}(t_0) = v(t_0)$

The error dynamics then take the form

$$M\Delta\dot{v} = M(\dot{\hat{v}} - \dot{v}) \quad (31)$$

$$= -\alpha M\Delta v - \Delta M\psi_2 - ad_{se(2)}(v)\Delta M v - W_{p_D}(v)\Delta\theta_{p_D} + W_{p_\mathcal{G}}(q)\Delta\theta_{p_\mathcal{G}} + G_a(\xi)\ \Delta\theta_a, \quad (32)$$

and we consider the Lyapunov function candidate

$$V(\Delta v, \Delta\theta_{pa}) = \frac{1}{2}\Delta v^T M\Delta v + \frac{1}{2\gamma_M}\Delta\theta_{p_M}^T\Delta\theta_{p_M} + \sum_{i=1}^{3}\frac{1}{2\gamma_{D_i}}\Delta\theta_{p_{D_i}}^T\Delta\theta_{p_{D_i}} + \frac{1}{2\gamma_\mathcal{G}}\Delta\theta_{p_\mathcal{G}}^T\Delta\theta_{p_\mathcal{G}} + \frac{1}{2\gamma_a}\Delta\theta_a^T\Delta\theta_a \quad (33)$$

which is positive definite in $\Delta v, \Delta\theta_{pa}$, radially unbounded, and equal to zero if and only if $\Delta v = 0$ and $\Delta\theta_{pa} = 0$. As in Section IV-A, we refer to the details of the proof in [3] to show that all signals remain bounded, $\dot{V}(t)$ is negative definite in Δv and negative semi-definite overall, $\lim_{t\to\infty}\Delta v(t) = \vec{0}$, $\lim_{t\to\infty}\dot{\hat{\theta}}_{pa}(t) = \vec{0}$ and $\lim_{t\to\infty}\hat{\theta}_{pa}(t) \in P$.

C. Simulation Results

We conducted a simulation study using the above 3-DOF model and the following conditions:

- AID gains:
  - $\alpha = 1.0$
  - $(\gamma_{P_M}, \gamma_{P_{D_1}}, \gamma_{P_{D_2}}, \gamma_{P_{D_3}}, \gamma_{P_\mathcal{G}}, \gamma_a) = (1.0, 20.0, 30.0, 40.0, 1.0, 50.0)$
- True parameters:
  - $\hat{\theta}_{p_M} = [1\ 0\ 1\ 1]^T$
  - $\hat{\theta}_{p_{D_1}} = [2\ 0\ 0\ 2\ 0\ 2]^T$
  - $\hat{\theta}_{p_{D_2}} = [3\ 0\ 0\ 3\ 0\ 3]^T$
  - $\hat{\theta}_{p_{D_2}} = [4\ 0\ 0\ 4\ 0\ 4]^T$
  - $m = 1.0$, $\rho_\bigtriangledown = 0.8$, $r_{cb} = [1\ 1.2]^T$
  - $\alpha_1, \alpha_2, \alpha_3 = 5.0$
  - $r_{a_1} = [-1\ -1]^T, r_{a_2} = [-1\ 1]^T, r_{a_1} = [1\ 0]^T$
  - $u_1 = [1\ 0]^T, u_2 = [1\ 0]^T, u_3 = [0\ 1]^T$
- Initial conditions:
  - $\hat{\theta_{p_M}} = [1\ 0\ 1\ 1]^T$
  - $\hat{\theta_{p_{D_i}}} = [1\ 0\ 0\ 1\ 0\ 1]^T$
  - $m = 1.1$, $\rho_\bigtriangledown = 0.8$, $r_{cb} = [1\ 1.2]^T$
  - $\alpha_1, \alpha_2, \alpha_3 = 1.0$
  - $r_{a_1} = [-1\ -1]^T, r_{a_2} = [-1\ 1]^T, r_{a_1} = [1\ 0]^T$
  - $u_1 = [1\ 0]^T, u_2 = [1\ 0]^T, u_3 = [0\ 1]^T$
- Control input:
  - $\xi_1 = sin(0.7t)$
  - $\xi_2 = sin(1.1t - \frac{\pi}{4})$
  - $\xi_3 = sin(2.0t - \frac{\pi}{3})$
- Error threshold: $\epsilon = 0.05$

which were chosen empirically such that initial parameter values different significantly from true parameters, gains provided reasonable convergence time, the error threshold resulted in consistent fault detection, and control input signals were smooth, bounded, and sufficiently rich to induce parameter convergence to P^*.

The NS-AID achieved convergence of velocity (Figure 2) and parameter estimates (Figure 3) over an interval of 1200 seconds. At t=1200 seconds, a fault consisting of a 50% decrease in the gain coefficient of the first thruster was introduced, corresponding for example to loss of a propeller blade. At t=2400 seconds, an additional fault representing loss of a streamlined hull fairing through a 150% scaling of the drag matrix of the second DOF was introduced. Both faults were followed by an immediate increase in the magnitude of $\Delta v(t)$ before the AID was able to attain new parameter estimates, after which $\Delta v(t)$ decreased to a near-zero value. Additionally, the magnitude of $\Delta v_{\theta_{pa^*}}(t)$ immediately increased after the introduction of a fault and remained nonzero, indicating persistence of the faults despite convergence of the NS-AID.

Figure 4 shows the output of the fault isolation algorithm, which correctly flagged the actuator parameters of the first fault and additionally flagged the drag parameters of the second fault while maintaining the status of the first fault. We observe that false fault detections occurred only sporadically and exclusively within the initial convergence period of each estimation interval. In practice, first performing fault detection using $\Delta v(t)$ and $\Delta v_{\theta_{pa^*}}(t)$ before attempting fault isolation would prevent erroneous results from applying the algorithm to badly-converged parameter estimates.

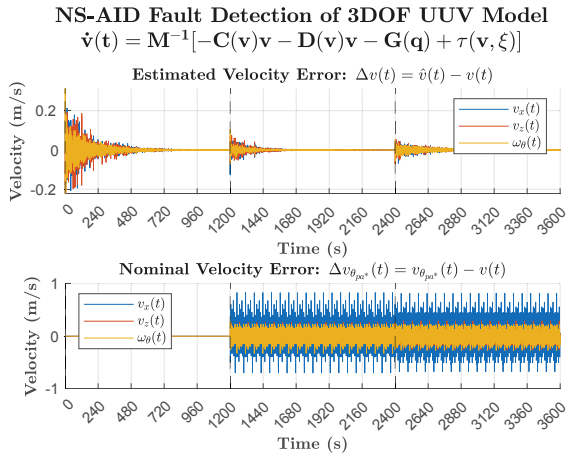

Fig. 2. The error $\Delta v(t)$ between the NS-AID estimated velocity and the true velocity (top) and the error $\Delta v_{\theta_{pa^*}}(t)$ between the velocity of a system under nominal parameters and the true velocity (bottom). The estimate error converges over each interval even after introducing faults at t = 1200 and t = 2400, while the nominal error indicates a persistence of fault behavior.

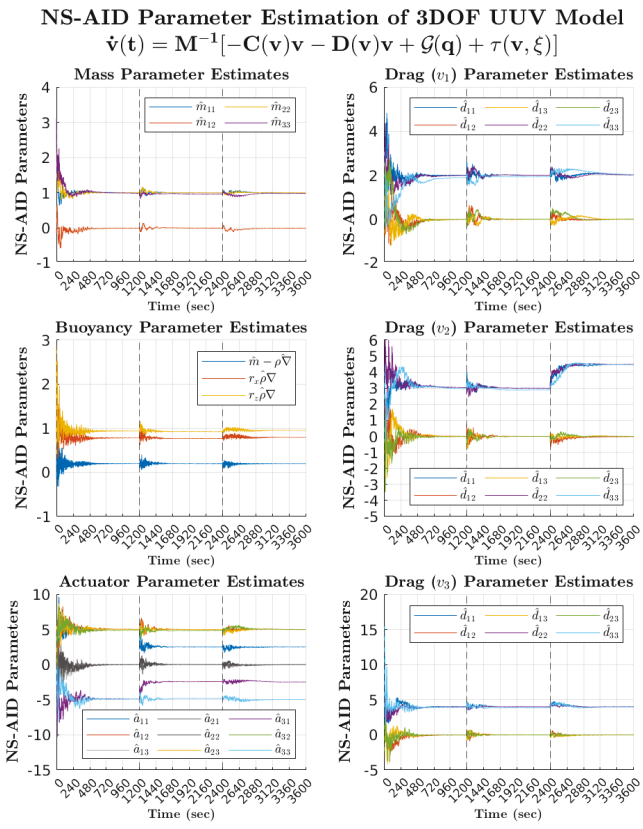

Fig. 3. Adaptively estimated parameters of the system, shown normalized by a scale factor to correspond to initial values of the "true" parameters. The first fault at t=1200 scales a_{11}, a_{21}, a_{31} by 50% (bottom left) and the second fault at t=2400 scales the second DOF drag by 150% (middle right).

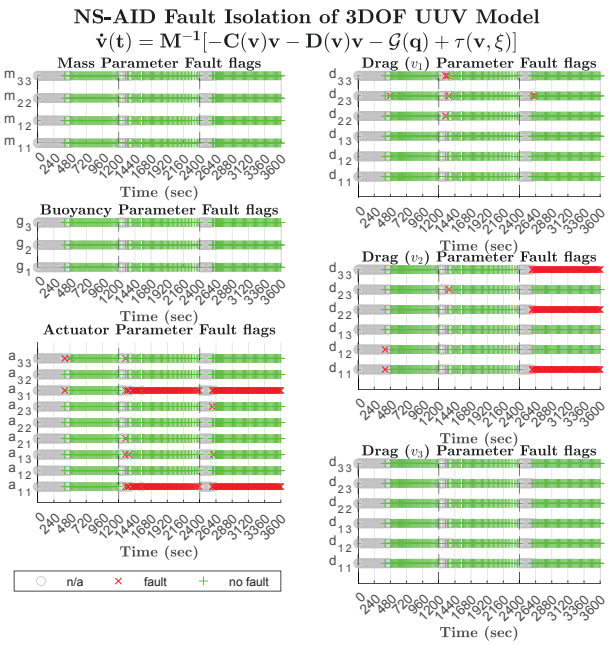

Fig. 4. The output of the fault isolation algorithm, which correctly identified no faults during the first interval, a two-parameter actuator fault during the second interval, and an additional three-parameter drag fault during the third interval. Scaled zero parameters were not flagged as faults.

Although these preliminary simulation results demonstrate FDI on a limited, fully-actuated model with simplified faults, they indicate the potential applicability of this approach to more complex 6-DOF models and fault scenarios.

VI. CONCLUSION

This paper has reported novel MB-FD and QS-FI approaches to the FDI problem for second-order nonlinear systems, as well as a preliminary numerical simulation evaluation of these approaches applied to a 3-DOF UUV plant model. The simulation study shows their ability to detect as well as isolate faults for the cases of both single and multiple simultaneous faults and suggests the generalizability of the MB-FD and QS-FI approaches to any well-defined second-order plant and actuator model whose parameters enter linearly: a broad class of systems which includes aerial vehicles, marine vehicles, spacecraft, and robot arms. Since the faults are not attached to any assumed fault model, but are characterized only from their effect on the vehicle dynamics, this approach shows significant potential for flexible and effective FDI. Moreover, obtaining an accurate estimation of true vehicle dynamics in the presence of faults forms a strong basis for fault-tolerant model-based control. In future work, we aim to address more complex 6-DOF plant models, underactuation, varied platforms including both marine and aerial vehicles, improvements in algorithmic efficiency, experimental evaluation incorporating more realistic model uncertainty, noise, and disturbance conditions, and comparative evaluation against current state-of-the-art FDI approaches.

REFERENCES

[1] National Research Council, Ocean Studies Board, Committee on an Ocean Infrastructure Strategy for U.S. Ocean Research in 2030, *Critical Infrastructure for Ocean Research and Societal Needs in 2030*. Washington, DC: The National Academies Press, 2011. https://doi.org/10.17226/13081.

[2] National Research Council, Ocean Studies Board, Committee on Guidance for NSF on National Ocean Science Research Priorities: Decadal Survey of Ocean Sciences, *Sea Change: 2015-2025 Decadal Survey of Ocean Sciences*. Washington, DC: The National Academies Press, 2015. https://doi.org/10.17226/21655.

[3] T. Paine, "Robust model identification methods for nonlinear second-order plant models for underwater vehicles," Master's thesis, Johns Hopkins University, 2018.

[4] Z. Gao, C. Cecati, and S. X. Ding, "A survey of fault diagnosis and fault-tolerant techniques—Part I: Fault diagnosis with model-based and signal-based approaches," *IEEE Transactions on Industrial Electronics*, vol. 62, pp. 3757–3767, June 2015.

[5] Z. Gao, C. Cecati, and S. X. Ding, "A survey of fault diagnosis and fault-tolerant techniques—Part II: Fault diagnosis with knowledge-based and hybrid/active approaches," *IEEE Transactions on Industrial Electronics*, vol. 62, pp. 3768–3774, June 2015.

[6] B. Y. Raanan, J. Bellingham, Y. Zhang, B. Kieft, M. J. Stanway, R. McEwen, and B. Hobson, "A real-time vertical plane flight anomaly detection system for a long range autonomous underwater vehicle," in *OCEANS 2015 - MTS/IEEE Washington*, pp. 1–6, Oct 2015.

[7] B. Y. Raanan, J. G. Bellingham, Y. Zhang, M. Kemp, B. Kieft, H. Singh, and Y. Girdhar, "Automatic fault diagnosis for autonomous underwater vehicles using online topic models," in *OCEANS 2016 MTS/IEEE Monterey*, pp. 1–6, Sept 2016.

[8] E. Baskaya, M. Bronz, and D. Delahaye, "Fault detection diagnosis for small UAVs via machine learning," in *2017 IEEE/AIAA 36th Digital Avionics Systems Conference (DASC)*, pp. 1–6, Sept 2017.

[9] C. N. Cho, J. T. Hong, and H. J. Kim, "Neural network based adaptive actuator fault detection algorithm for robot manipulators," *Journal of Intelligent & Robotic Systems*, vol. 95, no. 1, pp. 137–147, 2019.

[10] S. Vàsquez, M. Kinnaert, and R. Pintelon, "Active fault diagnosis on a hydraulic pitch system based on frequency-domain identification," *IEEE Transactions on Control Systems Technology*, vol. PP, no. 99, pp. 1–16, 2017.

[11] C. S. Jing, D. Pebrianti, G. M. Qian, and L. Bayuaji, "Fault detection in quadrotor MAV," in *2017 7th IEEE International Conference on System Engineering and Technology (ICSET)*, pp. 65–70, Oct 2017.

[12] J. Bellingham, "Fault detection, diagnosis, and mitigation for long-duration AUV missions with minimal human intervention," tech. rep., Monterey Bay Aquarium Research Inst., Moss Landing, CA, 2014. https://www.onr.navy.mil/reports/FY14/pobelli2.pdf.

[13] D. Yoerger, A. Bradley, B. Walden, M.-H. Cormier, and W. Ryan, "Fine-scale seafloor survey in rugged deep-ocean terrain with an autonomous robot," in *Proceedings 2000 ICRA. Millennium Conference. IEEE International Conference on Robotics and Automation. Symposia Proceedings (Cat. No.00CH37065)*, vol. 2, pp. 1787–1792, 2000.

[14] D. R. Yoerger, M. Jakuba, A. M. Bradley, and B. Bingham, "Techniques for deep sea near bottom survey using an autonomous underwater vehicle," *Int. J. Rob. Res.*, vol. 26, no. 1, pp. 41–54, 2007.

[15] J. C. Kinsey, D. R. Yoerger, M. V. Jakuba, R. Camilli, C. R. Fisher, and C. R. German, "Assessing the Deepwater Horizon oil spill with the *Sentry* autonomous underwater vehicle," in *Proc. IEEE/RSJ Intl. Conf. Intell. Robots Systems*, pp. 261–267, September 2011.

[16] D. R. Yoerger, "Personal communication," January 2014.

[17] M. Brito, D. Smeed, and G. Griffiths, "Underwater glider reliability and implications for survey design," *Journal of Atmospheric and Oceanic Technology*, vol. 31, no. 12, pp. 2858–2870, 2014.

[18] M. P. Brito, D. A. Smeed, and G. Griffiths, "Analysis of causation of loss of communication with marine autonomous systems: A probability tree approach," *Methods in Oceanography*, vol. 10, pp. 122 – 137, 2014. Special Issue: Autonomous Marine Vehicles.

[19] M. L. Seto and A. Z. Bashir, "Fault tolerance considerations for long endurance AUVs," in *2017 Annual Reliability and Maintainability Symposium (RAMS)*, pp. 1–6, Jan 2017.

[20] M.-A. Massoumnia, "A geometric approach to the synthesis of failure detection filters," *IEEE Transactions on Automatic Control*, vol. 31, no. 9, pp. 839–846, 1986.

[21] C. De Persis and A. Isidori, "A geometric approach to nonlinear fault detection and isolation," *IEEE Transactions on Automatic Control*, vol. 46, no. 6, pp. 853–865, 2001.

[22] T. Jiang, K. Khorasani, and S. Tafazoli, "Parameter estimation-based fault detection, isolation and recovery for nonlinear satellite models," *IEEE Transactions on Control Systems Technology*, vol. 16, no. 4, pp. 799–808, 2008.

[23] A. S. Rezazadeh, H. R. Koofigar, and S. Hosseinnia, "Adaptive fault detection and isolation for a class of robot manipulators with time-varying perturbation," *Journal of Mechanical Science and Technology*, vol. 29, no. 11, pp. 4901–4911, 2015.

[24] J. G. Graver, R. Bachmayer, N. E. Leonard, and D. M. Fratantoni, "Underwater glider model parameter identification," in *Proc. 13th Int. Symp. on Unmanned Untethered Submersible Technology (UUST)*, vol. 1, pp. 12–13, 2003.

[25] P. Ridao, A. Tiano, A. El-Fakdi, M. Carreras, and A. Zirilli, "On the identification of non-linear models of unmanned underwater vehicles," *Control Engineering Practice*, vol. 12, no. 12, pp. 1483–1499, 2004.

[26] Ø. Hegrenæs, O. Hallingstad, and B. Jalving, "Comparison of mathematical models for the HUGIN 4500 AUV based on experimental data," in *Symposium on Underwater Technology and Workshop on Scientific Use of Submarine Cables and Related Technologies.*, pp. 558 –567, April 2007.

[27] S. C. Martin and L. L. Whitcomb, "Experimental identification of six-degree-of-freedom coupled dynamic plant models for underwater robot vehicles," *IEEE Journal of Oceanic Engineering*, vol. PP, no. 99, pp. 1–10, 2013.

[28] Z. J. Harris, T. M. Paine, and L. L. Whitcomb, "Preliminary evaluation of null-space dynamic process model identification with application to cooperative navigation of underwater vehicles," in *2018 IEEE/RSJ International Conference on Intelligent Robots and Systems (IROS)*, pp. 3453–3459, IEEE, 2018.

[29] A. Tiano, R. Sutton, A. Lozowicki, and W. Naeem, "Observer Kalman filter identification of an autonomous underwater vehicle," *Control Engineering Practice*, vol. 15, no. 6, pp. 727–739, 2007.

[30] M. T. Sabet, H. M. Daniali, A. Fathi, and E. Alizadeh, "Identification of an autonomous underwater vehicle hydrodynamic model using the extended, cubature, and transformed unscented Kalman filter," *IEEE Journal of Oceanic Engineering*, vol. 43, no. 2, pp. 457–467, 2018.

[31] P. W. Van De Ven, T. A. Johansen, A. J. Sørensen, C. Flanagan, and D. Toal, "Neural network augmented identification of underwater vehicle models," *Cont. Eng. Prac.*, vol. 15, no. 6, pp. 715–725, 2007.

[32] G. C. Karras, C. P. Bechlioulis, M. Leonetti, N. Palomeras, P. Kormushev, K. J. Kyriakopoulos, and D. G. Caldwell, "On-line identification of autonomous underwater vehicles through global derivative-free optimization," in *2013 IEEE/RSJ International Conference on Intelligent Robots and Systems*, pp. 3859–3864, 2013.

[33] B. Wehbe, M. Hildebrandt, and F. Kirchner, "Experimental evaluation of various machine learning regression methods for model identification of autonomous underwater vehicles," in *IEEE International Conference on Robotics and Automation*, pp. 4885–4890, IEEE, 2017.

[34] N.-L. Wu, X.-Y. Wang, T. Ge, C. Wu, and R. Yang, "Parametric identification and structure searching for underwater vehicle model using symbolic regression," *Journal of Marine Science and Technology*, vol. 22, no. 1, pp. 51–60, 2017.

[35] D. A. Smallwood and L. L. Whitcomb, "Adaptive identification of dynamically positioned underwater robotic vehicles," *IEEE Transactions on Control Systems Technology*, vol. 11, no. 4, pp. 505–515, 2003.

[36] C. J. McFarland and L. L. Whitcomb, "Stable adaptive identification of fully-coupled second-order 6 degree-of-freedom nonlinear plant models for underwater vehicles: Theory and experimental evaluation," *International Journal of Adaptive Control and Signal Processing*, vol. 35, no. 5, pp. 786–810, 2021.

[37] S.-E.-I. Hasseni and L. Abdou, "Adaptive nonlinear robust control of an underactuated micro UAV," *International Journal of Dynamics and Control*, pp. 1–23, 2021.

[38] O. Egeland and J.-M. Godhavn, "Passivity-based adaptive attitude control of a rigid spacecraft," *IEEE Transactions on Automatic Control*, vol. 39, no. 4, pp. 842–846, 1994.

[39] H. F. Al-Shuka and R. Song, "Hybrid regressor and approximation-based adaptive control of robotic manipulators with contact-free motion," in *2018 2nd IEEE Advanced Information Management, Communicates, Electronic and Automation Control Conference (IMCEC)*, pp. 325–329, IEEE, 2018.

[40] K. Narendra and A. Annaswamy, *Stable Adaptive Systems*. NY: Dover Publications, 2005.

[41] S. Sastry and M. Bodson, *Adaptive Control: Stability, Convergence, and Robustness*. Prentice-Hall, 1989.